Applied Catalysis B: Environmental 241 (2019) 521–527

Contents lists available at ScienceDirect

Applied Catalysis B: Environmental

journal homepage: www.elsevier.com/locate/apcatb

Promoting electrocatalytic overall water splitting with nanohybrid of transition metal nitride-oxynitride

Soumen Dutta[a,b], Arindam Indra[b], Yi Feng[a], HyukSu Han[c], Taeseup Song[a,*]

[a] Department of Energy Engineering, Hanyang University, Seoul, 133-791, Republic of Korea
[b] The Research Institute of Industrial Science, Hanyang University, Seoul, 133-791, Republic of Korea
[c] Korea Institute of Industrial Technology, 137-41 Gwahakdanji-ro, Gangneung-si, Gangwon, 25440, Republic of Korea

ARTICLE INFO

Keywords:
Water-splitting
Electrocatalyst
Metal nitride-oxynitride
Nanohybrid
Low overpotential
Bifunctionality

ABSTRACT

Excellent Electrochemical water splitting with remarkable durability can provide a solution for the increasing global energy demand. Herein, we report an efficient and stable overall water splitting system; cobalt nitride-vanadium oxynitride nanohybrid, prepared from the polyaniline (PANI) mediated synthetic protocol. This nanohybrid produces significantly higher water oxidation, proton reduction as well as overall water splitting performances compared to the cobalt nitride, vanadium oxynitride or even noble metal catalyst systems. Only 263 mV overpotential is required to reach 10 mA cm^{-2} current density for oxygen evolution reaction (OER) and 118 mV for the same in case of hydrogen evolution reaction (HER). Finally, the bifunctional nanohybrid has been explored for the alkaline overall water splitting at cell voltage of 1.64 V to attain 10 mA cm^{-2} current density with long term stability for 100 h. Post-catalytic analyses have revealed the formation of defect rich amorphous CoO_x sites leading to high OER activity, whereas crystalline $Co(OH)_2$-Coδ^+-N ($0 < \delta < 2$) centres are generated after HER. To the best of our knowledge, this is the first example of a nitride-oxynitride nanohybrid system employed for the overall water splitting, and its superior activity and durability recommend its potential for practical utilization.

1. Introduction

The ever increasing energy demands, depletion of fossil fuels as well as their negative impacts on environment seek the urgency towards the exploration of alternative renewable energy resources [1–3]. Importantly, hydrogen is considered to be the most ideal future generation sustainable energy source. The major challenge for the hydrogen evolution reaction (HER) through electrochemical water splitting depends on the other kinetically sluggish counter reaction, i.e., oxygen evolution reaction (OER) [2]. Though, noble metal catalyst systems produced reasonable activity in HER and OER, their high cost, low stability and scarcity have restricted their practical application [3]. In this respect, first row transition metal based catalysts have been recently explored for either OER or HER [4–6]. Use of a single bifunctional catalyst for both OER, HER as well as overall water splitting is rare and requires special attention due to the use of a common electrolyte solution for effective performance in both the half-cell reactions [7,8]. Transition metal sulphides, selenides and phosphides have been developed in last few years for the efficient overall water splitting [8–10]. The low stability of these catalysts for the long term electrochemical performance is a serious concern for the practical use.

In contrast, metal nitrides and oxynitrides are well known for their high conductivity and improved corrosion resistant property, which are highly important for outstanding activity and durability during electrochemical test [11–14]. Moreover, the introduction of N atoms changes the electronic environment around the metal centres resulting in structural modification and easy charge transfer [14]. Although, a series of transition metal nitrides such as cobalt nitrides, nickel nitrides etc. have been explored for OER [15–19] or HER [20–24], their use for the overall water splitting is relatively unexplored to the best of our knowledge [25–28]. It should be mentioned here that the incorporation of a second metal in the electrocatalysts increases the number of active sites, reduces the charge transfer resistance and hence a notable improvement in the electrochemical performances is observed [25–28]. Earth abundant vanadium with multi valences (II−V) was found to be effective to provide required electronic and structural environment for the improved activity from cobalt and nickel based materials during electrochemical water oxidation [29–31]. However, their performance could further be enhanced through nitrogen incorporation into the metals for requisite d-band contraction to enhance the electron density

* Corresponding author.
E-mail address: tssong@hanyang.ac.kr (T. Song).

https://doi.org/10.1016/j.apcatb.2018.09.061
Received 11 January 2018; Received in revised form 1 September 2018; Accepted 18 September 2018
Available online 22 September 2018
0926-3373/

just below the Fermi level [14,32,33]. Thus more metallic character and easy electron transportation on the catalyst surface with large number of catalytically active sites in bimetallic nitride/oxynitride system could be the ideal substrate for the sustainable energy conversion.

Looking at this point, we have developed cobalt nitride (Co_4N) on carbon cloth (CC) and employed for both H_2 and O_2 evolution. A significant improvement in the bifunctional electrocatalytic activity has been achieved for the first time with vanadium incorporation in the system to produce a nanohybrid of Co_4N-vanadium oxynitride ($VN_{1-x}O_x$). Additionally, the current report is crucial in terms of avoiding direct use of toxic ammonia gas for metal nitride formation [15,16,33], rather pyrolyzation of nitrogen rich compounds [17,24] on carbon cloth based precursor is found to be sufficient to obtain the desired material. Herein, an integrated three dimensional Co_4N-$VN_{1-x}O_x$ architecture (CVN/CC) is fabricated by pyrolyzing Co-V precursor grown on polyaniline (PANI) coated CC i.e., CV-PANI/CC. The prepared metal nitride-oxynitride nanohybrid exhibits outstanding electrocatalytic performance by showing only 263 and 118 mV overpotential to achieve 10 mA cm^{-2} current density for OER and HER, respectively in 1.0 M KOH. In addition, only 1.64 V cell voltage is required for the material to get 10 mA cm^{-2} current density during alkaline water splitting in two electrode-system with a remarkable 100 h long stability.

2. Experimental section

2.1. Materials

All the reagents used were of analytical reagent (AR) grade and used as received without any further purification. Ammonium peroxodisulfate (APS), aniline (≥ 99.5%), cobalt nitrate [$Co(NO_3)_2.6H_2O$], vanadyl sulfate ($VOSO_4{\cdot}xH_2O$), urea [$CO(NH_2)_2$], ammonium fluoride (NH_4F), RuO_2, 20% Pt/C and nafion (5%) were purchased from Sigma-Aldrich. Hydrochloric acid (HCl) and potassium hydroxide (KOH) pellet were bought from Daejung, Korea whereas carbon cloth (CC) was obtained from MTI Korea. Deionised water was used throughout the course of the investigation.

2.2. Synthesis of polyaniline coated carbon cloth (PANI/CC)

The preparation of PANI/CC was achieved via ammonium persulfate (APS) mediated polymerization of aniline [34] in presence of one piece (2 cm × 3 cm) of pre-treated CC (See Supporting Information for experimental details for treatment of CC). In a typical synthetic process, 1.15 g of APS was dissolved in 50 mL 1.0 M HCl, followed by dropwise addition of 0.4 mL of aniline for 30 min while maintaining the temperature at ~5 °C. Then the whole mixture was kept stirring for overnight at room temperature. Finally, the PANI/CC was washed thoroughly with deionized water and dried at 60 °C before further use.

2.3. Synthesis of cobalt-vanadium precursor on PANI/CC (CV-PANI/CC)

The polyaniline (PANI) coated CC (2 cm × 3 cm) was immersed into 18 mL aqueous solution containing 3.0 mmoL $Co(NO_3)_2.6H_2O$, 1.5 mmoL $VOSO_4{\cdot}xH_2O$, 10.0 mmoL NH_4F and 20.0 mmoL $CO(NH_2)_2$ in 50 mL Teflon-lined stainless-steel autoclave for hydrothermal reaction at 150 °C for 20 h. The resulting product, CV-PANI/CC was collected, subsequently rinsed with deionized water and finally dried at 60 °C for overnight.

2.4. Synthesis of cobalt vanadium nitride on CC (CVN/CC)

To prepare the mixed metal nitride, the as-synthesized CV-PANI/CC substrate was calcined at 700 °C for 2.5 h with a heating speed of 4 °C min^{-1} under argon (Ar) environment (30 sccm) then cooling down naturally to room temperature before use.

2.5. Synthesis of CVN-NH_3/CC

First, CV/CC was synthesized from the same reaction protocol as described for CV-PANI/CC except the use of bare CC in the reaction mixture instead of PANI-CC. Then the freshly prepared CV/CC substrate was placed in a tube furnace and heated at 420 °C at 5 °C min^{-1} under a constant flowing NH_3 atmosphere (100 sccm) for 2.5 h and then cooling down naturally to room temperature.

2.6. Electrochemical studies

The electrocatalytic studies were performed in Autolab potentiostat/galvanostat (Model PGSTAT-72637) workstation using three-electrode configuration at ambient temperature. The as-fabricated carbon cloth based materials were directly used as the working electrode while a platinum disc electrode (1 cm^2) as the counter electrode and Ag/AgCl (KCl saturated) as the reference were employed. For the investigation of HER and OER by various electrocatalysts, linear sweep voltammetry (LSV) was conducted at a scan rate of 2 mV s^{-1} in Ar-saturated 1.0 M KOH (pH ≈ 13.6). Electrochemical impedance spectroscopy (EIS) was performed in a frequency range of 0.01 Hz–10^5 Hz with 5 mV amplitude at a bias potential of −0.19 and 1.56 V (vs. RHE) for HER and OER, respectively. All potentials reported in this paper were normalized with respect to the reversible hydrogen electrode (RHE) by adding a value of (0.21 + 0.059 × pH) V. Overall water splitting was carried out in a two-electrode cell using same catalyst as both the cathode and anode in Ar-saturated 1.0 M KOH.

2.7. Preparation of standard electrodes

For the comparison of HER, OER and overall water splitting with commercially available standardized materials, Pt-C and RuO_2 were coated on carbon cloth with ~2 mg cm^{-2} mass loading. In particular, 10.31 mg of Pt/C or 2.14 mg of RuO_2 was dispersed in 950 µL ethanol-water mixture (1:1), and 50 µL 1.0% nafion under strong ultra-sonication for 1 h. Next, the obtained suspensions were coated on carbon cloth (1 cm^2) separately and dried under ambient condition before use.

3. Results and discussion

3.1. Material characterizations

Scheme 1 represents the synthetic protocol for Co_4N-$VN_{1-x}O_x$ nanohybrid on carbon cloth (CVN/CC) through adopted polyaniline (PANI) induced synthetic strategy. This procedure avoids the direct use of toxic ammonia gas as well as results in the evolution of nitrogen

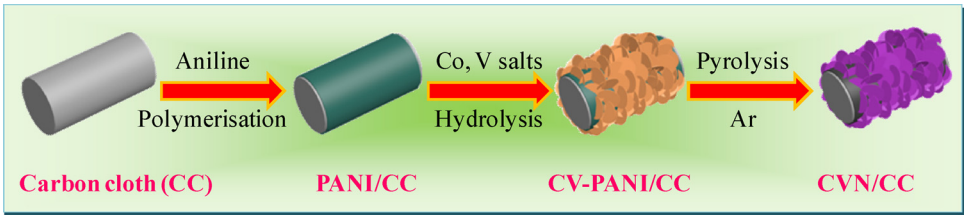

Scheme 1. Schematic representation for the synthesis of CVN/CC.

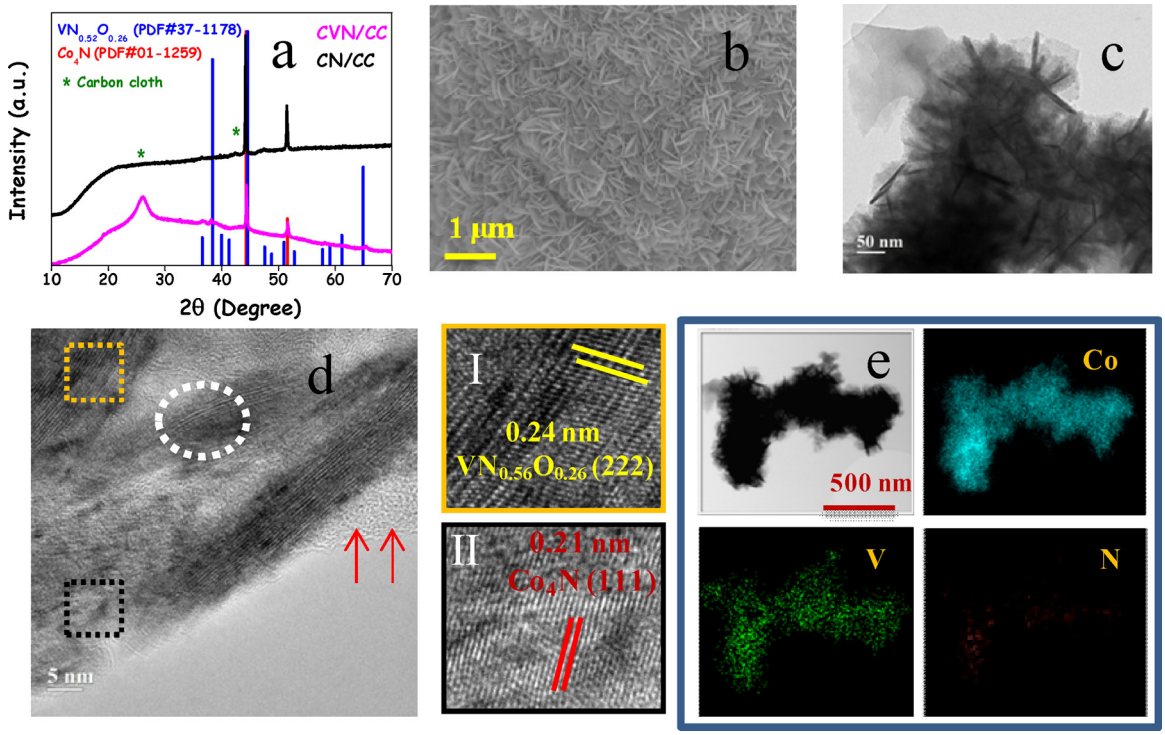

Fig. 1. (a) Comparative XRD pattern for CVN/CC and CN/CC, (b) FESEM, (c) TEM, (d) HRTEM, (e) elemental mapping for CVN/CC.

doped carbon layers in between the catalyst and CC ensuring better electrochemical activity and stability. First, oxidation promoted polymerization of aniline was employed to form PANI on carbon cloth, (Fig. S1) followed by the deposition of metal hydroxides (Fig. S2) and subsequent annealing in argon atmosphere at 700 °C to get the nitride and/or oxynitride system. The powder X-ray diffraction (PXRD) patterns of CVN/CC represents a mixture of cubic phases Co_4N (JCPDS; 01-1259) and $VN_{1-x}O_x$ (JCPDS: 37-1178) whereas PXRD of the vanadium free CN/CC clearly shows the formation of phase pure Co_4N (Fig. 1a) and cobalt free VN/CC matches with the mixture of $VN_{1-x}O_x$ (JCPDS 37-1178) and V_2O_3 (JCPDS 39-0774) (Fig. S3).

Field emission scanning electron microscopy (FESEM) studies of CVN/CC-700 demonstrate the perpendicular growth of CVN nanoflake array on carbon cloth (Figs. 1b, S4a). Transmission electron microscopy (TEM) analyses reveal the lamellar morphology of CVN to form flower-like structure (Figs. 1c, S4b). In addition, the dark centres of the flowers represent about the strong attachment of the individual nanoflakes, whereas nearly transparent nature of the flakes are clearly observable at the edges of the flowers. High-resolution TEM (HRTEM) studies show two different lattice fringe spacing; 0.21 nm and 0.24 nm corresponding to Co_4N (111) and $VN_{1-x}O_x$ (222), respectively (Fig. 1d). In addition a predominant amount of lattice defects in the material is clearly visible (white dotted circle) with the presence of amorphous N-doped carbon formed by the carbonization of PANI as indicated by red arrows (see more description in Fig. S5). The homogeneous distribution of Co and V confirms the formation of cobalt nitride and vanadium oxynitride nanohybrid in CVN/CC (Fig. 1e). FESEM images of CN/CC show well deposition of the nitride materials on CC with aggregated particles whereas VN/CC grows as a flake like structure (Fig. S6). High magnification image suggests that the flakes are highly porous in nature.

Further, X-ray photoelectron spectroscopic (XPS) studies of CVN/CC have been carried out to get insight of the valence states and the electronic structure of the elements on the surface of the catalyst (Fig. 2). The deconvoluted Co $2p_{3/2}$ peak clearly illustrates the presence of Co^{2+}-N (780.5 eV) and Co^{3+}-N (782.8 eV) (Fig. 2a) [23,27]. Additionally, satellite peaks at 785.6 eV and 789.2 eV represents the mixed valence state of cobalt. The V $2p_{3/2}$ XPS spectrum in Fig. 2b suggests the presence of V^{4+} (516.3 eV) and V^{5+} (517.3 eV) with small amount of V^{3+} (515.3 eV) oxidation state [13]. It is worth mentioning that we used PANI as nitridation source and in-turn it has been converted to nitrogen doped carbon on the surface of carbon cloth along with the generation of metal nitrides. The N 1 s XPS spectrum (Fig. 2c) has been indexed into six different peaks related to Co-N (397.9 eV), pyridinic N (398.3 eV), pyrrolic N (399.7 eV), V-N-O (399.3 eV), quaternary N (400.7 eV), pyridinic N-oxide (403.0 eV) [15,35–38]. In addition, C 1s XPS spectrum also contains significant contribution from C–N (285.7 eV) and C=N (287.3 eV) in association with graphitic carbon (284.5 eV) [37]. Moreover, O 1 s spectrum represents metal-oxygen bonding (529.6 eV) for $VN_{1-x}O_x$, dissociative adsorbed oxygen i.e., O_{ads} (531.1 eV) and unavoidable adsorbed water (533.6 eV) as shown in Fig. 2e [27,28]. Details XPS analyses of CN/CC and VN/CC are discussed in Fig. S7.

3.2. Electrocatalytic oxygen evolution reaction (OER) and hydrogen evolution reaction (HER) studies

Next, the well characterized materials have been investigated for the electrochemical water oxidation in 1.0 M aqueous KOH solution. The best catalytic activity was obtained with CVN/CC which produced 10 mA cm^{-2} current density at overpotential (η_{10}) of 263 mV (Fig. 3a). The performance of CVN/CC is superior to synthesized CN/CC (η_{10} = 327 mV), recently reported Co-VN catalyst (η_{10} = 320 mV) [33] and even outperformed state of the art noble metal catalyst RuO_2/CC (η_{10} = 295 mV), proving the high performance of the hybrid nitride-oxynitride system. The faster OER kinetics of the CVN/CC is reflected in the smaller Tafel slope of 64.1 mV dec^{-1} compared to pure cobalt nitride (99.2 mV dec^{-1}) (Fig. 3b) [39]. The faster charge transfer of the CVN/CC compared to the other materials is also confirmed by the smallest semi-circle obtained from the electrochemical impedance (EIS) measurements (Fig. S8) [15–25]. The charge transfer resistance (R_{ct}) value follows the trend: CVN/CC (1.6 Ω) < RuO_2/CC (2.7 Ω) < CN/CC (3.4 Ω). Chronoamperometric (CA) measurement at 1.56 V vs RHE was carried out to estimate the stability of the materials (inset; Fig. 3b). The obtained current density (~14.4 mA cm^{-2}) from the designed

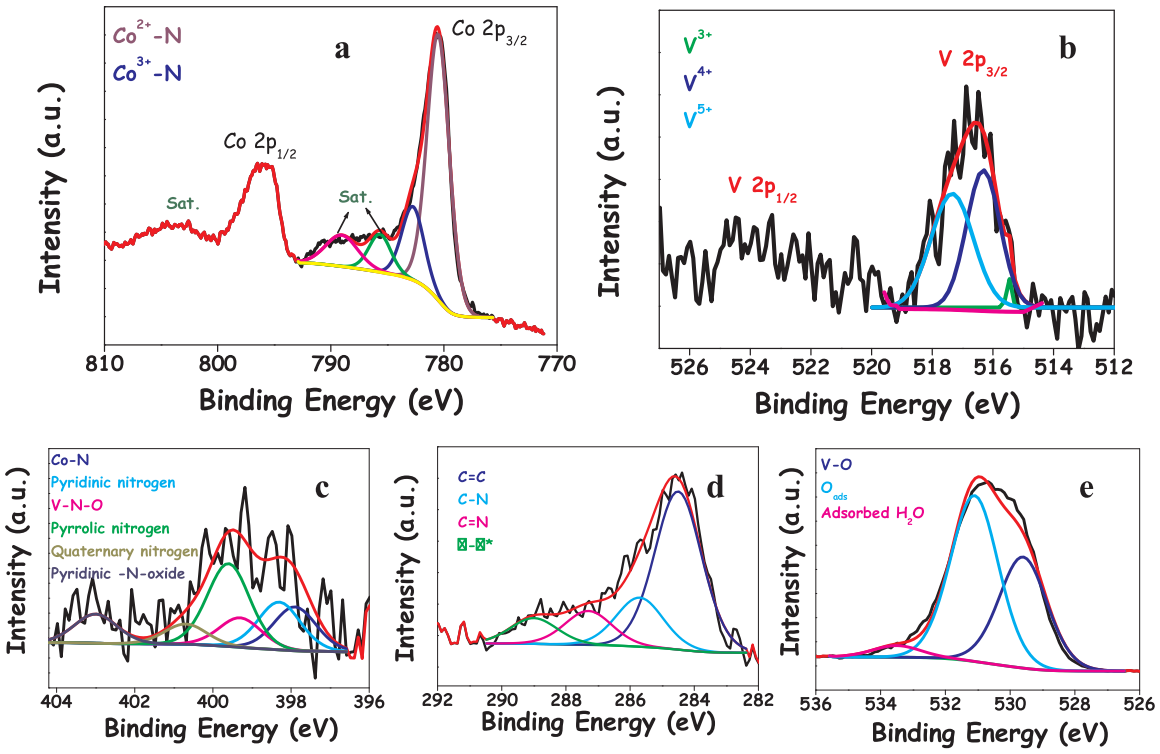

Fig. 2. XPS spectra for (a) Co 2p, (b) V 2p, (c) N 1s, (d) C 1s and (e) O 1s in CVN/CC.

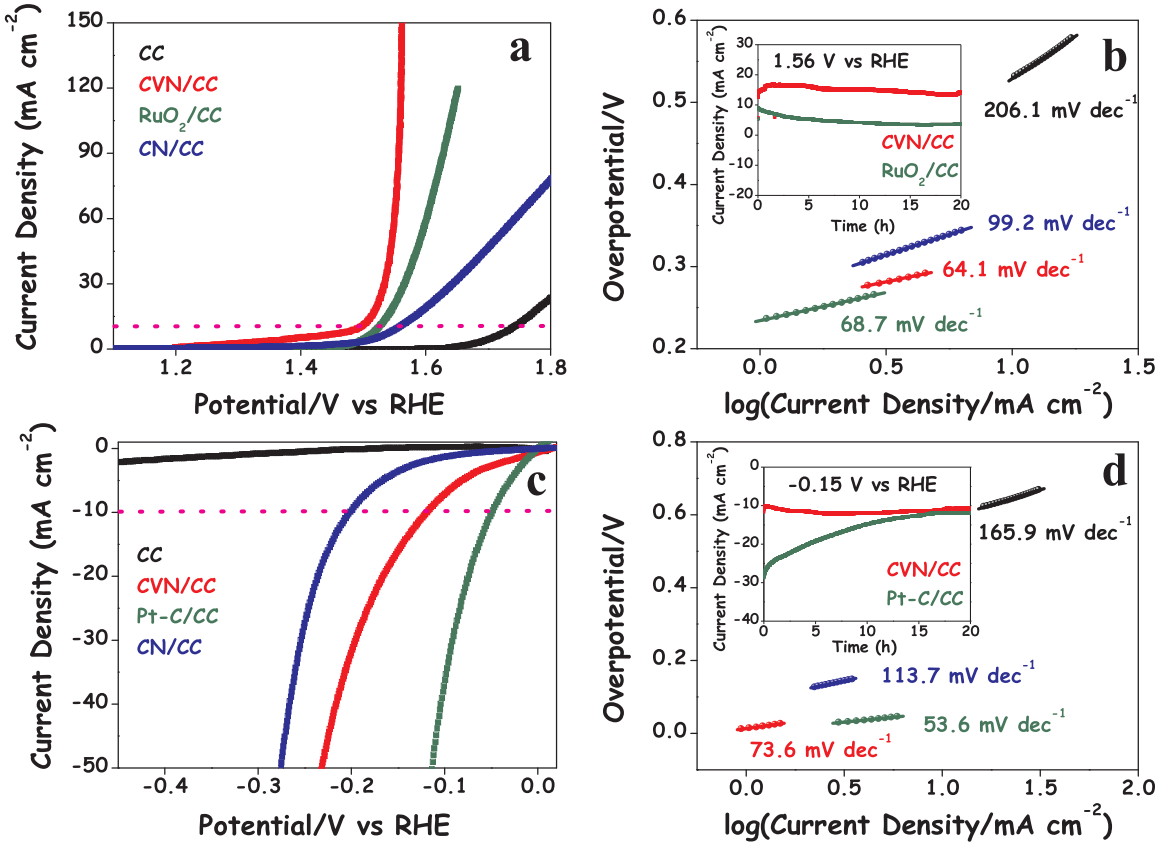

Fig. 3. Comparative (a) *iR*-corrected LSV profiles and (b) Tafel plots (inset: CA test at 1.56 V vs RHE) for OER tested catalysts; comparative (c) *iR*-corrected LSV profiles and (d) Tafel plots (inset: CA test at −0.15 V vs RHE) for HER tested catalysts.

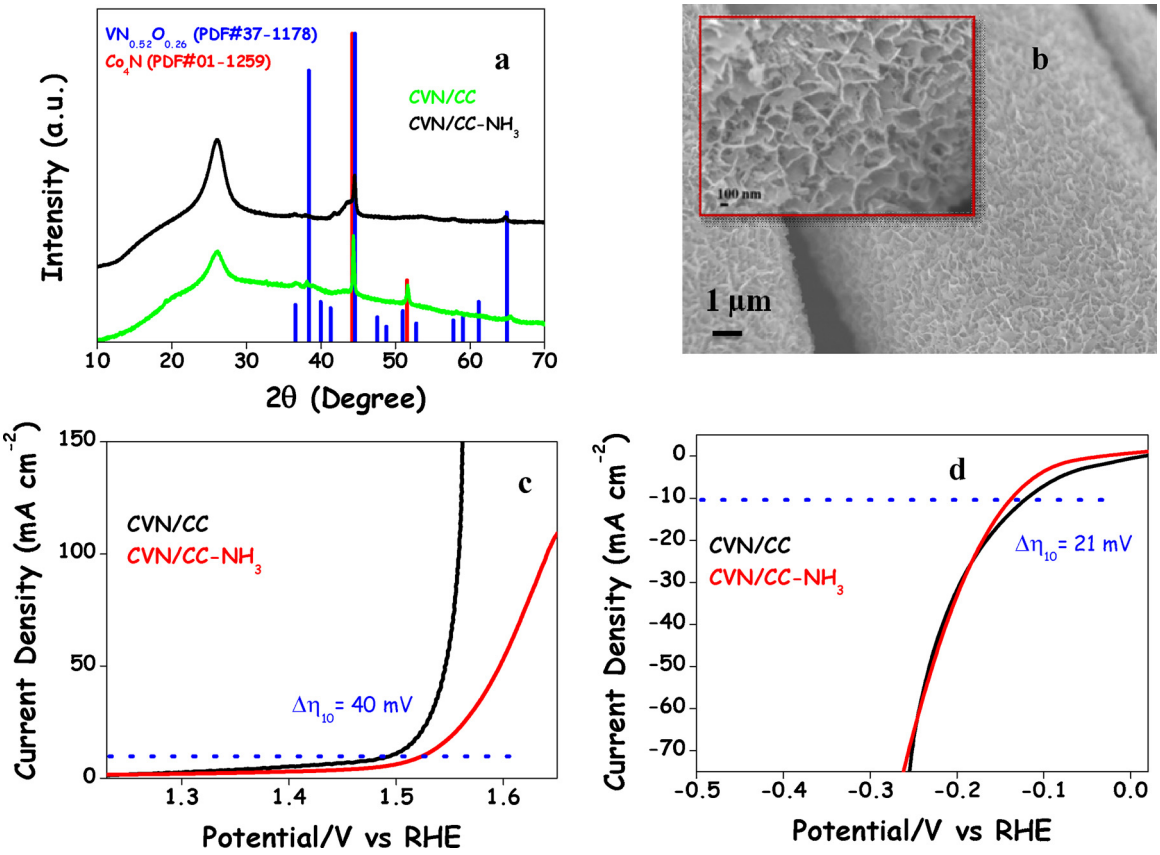

Fig. 4. (a) Comparative XRD pattern of PANI derived CVN/CC and CVN/C C-N H_3, (b) FESEM images of CVN/C C-N H_3, comparative (c) OER and (d) HER performance between CVN/CC and CVN/C C-N H_3 in 1.0 M KOH solution.

CVN/CC catalyst was found to be increased during CA testing for initial 5 h and reaches to 16.3 mA cm^{-2}. Finally, it generates 15.2 mA cm^{-2} current density after 20 h of CA study. The initial increment in the current density can be explained by the formation of the new active sites for the catalysis during electrochemical activation of the catalyst. The decrease in the current density with time is due to the partial deactivation of the active sites as well as detachment of the catalyst from CC support. However, the material was able to produce similar current density after 20 h CA test while compared to initial performance. In contrast, the fabricated RuO_2/CC failed to show such behaviour rather it lost 60% initial activity within the same time period. In addition, Faradaic efficiency (FE) of CVN measured during OER is found to be 99.9% as described in Fig. S9.

Further, proton reduction activities of the designed materials have been tested by linear sweep voltammetric (LSV) studies in 1.0 M KOH. The LSV profiles clearly reveal better HER performance of CVN/CC compared to CN/CC with much lower overpotential (118 mV vs. 201 mV) for 10 mA cm^{-2} current density (Fig. 3c). The Tafel slopes indicate the favored kinetics for HER with CVN/CC (73.6 mV dec^{-1}) compared to CN/CC (Fig. 3d). The Tafel slope value for CVN/CC suggests that the HER proceeds through Volmer-Heyrovsky mechanism i.e., the initially formed adsorbed hydrogen atom (H_{ads}) accepts an electron and then combines with water molecule to discharge as H_2 [40]. In addition, the exchange current density (J_0; Current density at zero overpotential) is calculated to be 0.65, 0.21 and 0.85 mA cm^{-2} from the Tafel plot for CVN/CC, CN/CC and Pt-C/CC, respectively. The favorable reaction kinetics in CVN/CC can be explained from its lower charge transfer resistance (1.71 Ω) compared to CN/CC (3.19 Ω) as illustrated in the EIS plot recorded at -0.19 V vs. RHE (Fig. S8b). Importantly, in the CA test at −0.15 V vs RHE, CVN/CC demonstrates slight activity enhancement (from −10.7 to −12.05 mA cm^{-2} after 7 h) like OER case in the initial period and finally it produces a current density of -10.7 mA cm^{-2} after 20 h. Although, the HER activity of CVN/CC is lower than Pt-C/CC, its stability is far better than the commercial Pt-C/CC catalyst which looses ~58% initial activity after 20 h of CA test (inset; Fig. 3d).

The fundamental aspects for the newly synthesized water splitting catalysts lie on their high efficiency, longer lifetime and lower cost for practical consumption. Detailed studies of OER and HER performance by CVN/CC disclose it's prospective as an outstanding substitute of the expensive catalysts in terms of better or comparable activity, but most importantly with superior stability. It is worth mentioning that self-supported nature of this designed material reduces the production cost, enables efficient mass and electron transfer process for the enhancement in electrocatalytic activity and also its strong integration on the support leads to improved stability. The presence of V plays the major role for tremendous enhancement in catalytic activities in CVN/CC due to facile charge transfer process and assisting easy transformation of Co centers into catalytically active species [27]. Variation in the ratio of Co/V significantly affects the OER and HER performance and presence of vanadium with optimum amount in mixed metal nitride results in enhanced electrocatalytic activity (Fig. S10, S11). Moreover, electrochemically active surface area (ECSA) of CVN/CC is found to be 1.21 times higher than that of CN/CC demonstrating availability of more active sites in CVN/CC with introducing second metal in catalyst structure (Fig. S12a–c). Previously, OER improvement by the incorporation of Fe, Mn and V have been reported, [10,25–29] but prominent effect of $VN_{1-x}O_x$ on cobalt nitride for both OER and HER is hitherto new and important. Even, specific activity (ECSA normalized) of CVN/CC for OER and HER is superior to CN/CC suggesting improved intrinsic property with the introduction of V (Fig. S12d, e) in the current nanohybrid. Here it is important to note that the catalytic activity of VN/CC and nitrogen doped carbon on CC (N_x-C/CC) is far behind CVN/CC as more potential is required to reach 10 mA cm^{-2} current

density for both OER and HER (Fig. S13). In addition, CVN/CC electrocatalyst prepared at higher temperature (800 °C) forms aggregated structures and also produces lower water splitting activity compared to the catalyst prepared at 700 °C (Fig. S14).

In order to establish the importance of our developed protocol to fabricate mixed metal nitride, we have also prepared to same CoV nitride following the common practice i.e., using toxic ammonia (NH_3) gas for the nitridation [19,27]. XRD profile of the CVN/C C-N H_3 resembles with our desired material CVN/CC as shown in Fig. 4a. FESEM image indicates that CVN/C C-N H_3 material is composed of a large number of two dimensional nanosheets (Fig. 4b) as well as porous architecture at their surface (Inset; Fig. 4b). Comparative OER and HER results disclose that PANI-induced synthesis of CoV nitrides on CC are more active than CVN/C C-N H_3 as shown in Fig. 4c–d. The PANI coated on CC has two important roles to play; designing of CVN nanoarchitecture and improving the electrochemical performance. PANI influences the deposition of the metal hydroxides as well as controls their growth on CC. Inductively coupled plasma optical emission spectrometry (ICP-OES) result reveals that catalyst loading in CVN/CC is almost 1.5 times higher than CVN/C C-N H_3 (Table S1 and S2), which has been reflected in their HER and OER performances. Another favorable outcome of the PANI derived materials appear from the development of nitrogen doped carbon in between the catalyst and CC during thermal treatment of PANI (Fig. S5). This conducting N-doped carbon layers have assisted the charge transfer process and hence the water splitting activity, proving the importance of our synthetic strategy [41–43]. Table S1 represents comparative account on catalyst loading and electrochemical performances of the synthesized materials in this study.

3.3. Full water splitting in two-electrode system

Inspired by the outstanding bifunctional characteristic of CVN/CC in HER and OER compared to previous reports (Table S3, S4), a two-electrode electrolyzer was assembled and tested for the overall water splitting. Only 1.64 V cell potential is required to attain the current density of 10 mA cm^{-2} (Fig. 5a). This performance is superior to CN/CC (1.78 V) and even comparable to commercial RuO_2/CC and Pt-C/CC couple (1.65 V). Here, it is important to note that CVN/CC material is one of the leading electrocatalysts while compared with the recently reported noble metal free bifunctional catalysts including Fe_2Ni_2N/NF (1.65 V) [25], $NiFe_3N$/NF (1.62 V) [26], V/NF (1.74 V) [35], VOOH/NF (1.62 V) [44], Co_1Mn_1CH/NF (1.68 V) [45], Co-S/CTs/CP (1.74 V) [46], $Co_{0.85}Se$/NiFe-LDH/EG(1.67 V) [47], Ni_5P_4/ Ni foil (1.70 V) [48], $NiMoP_2$/CC (1.67 V) [49], Ni-Co-B/NF (1.72 V) [50], NiCoP/Ti (1.64 V) [51], NiFe nanosheets/$NiCo_2O_4$ nanoflakes/NF (1.67 V) [52], $NiCo_2O_4$/NF (1.65 V) [53], CoP/CoP_2/Al_2O_3/CP (1.65 V) [54], Ni_3Se_2/Co_9S_8/EG (1.62 V) [55] and so on (Table S5). Moreover, a remarkable retention of the initial activity (~90%) after 100 h of CA measurement was found for CVN/CC compared to poor stability performance of the commercial couple after 6 h study (Figs. 5b and S15).

3.4. Post-catalytic structural analyses of CVN/CC

Further, we have analyzed CVN/CC catalyst after OER and HER to investigate its structural and compositional change during water splitting. FESEM images after prolong CA suggest the robustness and strong mechanical stability of the self-supported catalyst as the carbon cloth is well covered with the material (Fig. S16). Although ICP-OES results indicate the significant leaching of V during OER and HER, the Co content remains almost unchanged in the matrix (Table S2). HRTEM analyses after OER revealed a complete amorphization [56] of the catalyst unlike only at the surface reported for the transition metal based catalysts (Fig. S17a) [16]. In addition, leaching of V leads to the generation of cationic vacancy in the structure of the active catalyst and enhances the porosity of the two dimensional structure (Fig. S17b). This indeed improves the charge transport and mass transfer by promoting the OER performance as found in the initial enhancement of the anodic current during CA investigation. On the contrary, the post-HER catalyst is found to be highly crystalline and observed lattice spacing value of 0.238 nm is well matched with the (101) plane of generated $Co(OH)_2$ (Fig. S17c,d) [57].

XPS investigation of the post-catalysis material further confirms its transformation and reveals about its new composition. Post-OER catalyst material shows that the intensity of the peak for Co^{2+}-N was reduced with the appearance of various oxygenated Co species such as Co^{3+}-OOH, Co^{2+}-OH (Fig. S18) [10,56]. In addition, the spin-orbit level energy spacing between Co $2p_{3/2}$-Co $2p_{1/2}$ reduced to 15.3 eV after CA from 15.7 eV in fresh catalyst. This result confirms the oxidation of Co^{2+} to Co^{3+} to form hydroxide-oxyhydroxide structure during OER [15,50,56]. On the other hand, the XPS peak corresponding to Co^{2+}-N after HER is shifted to lower binding energy (0.9 eV) probably due to transformation into lower oxidation states of $Co\delta^+$-N ($0 < \delta < 2$) i.e., metallic character in Co centers is increased [58,59]. Additionally, the peak for Co^{3+}-N is found to be vanished completely and unavoidable formation of $Co(OH)_2$ (ca. Co $2p_{3/2}$ = 781.2 eV) in alkaline medium is also found [57,60]. The transformation of nitrides into metal oxides/hydroxides in alkaline medium is further proved in almost vanished N 1 s XPS spectra as well as large response from metal-oxygen bond in the O 1 s XPS spectra. Therefore, the transformation of Co_4N-$VN_{1-x}O_x$ into amorphous cobalt oxo-hydroxide species i.e., CoO_x through the possible leaching of V in alkaline medium is the main contributing factor for high OER performance [61,62]. On the other hand, in-situ generated crystalline $Co(OH)_2$-$Co\delta^+$-N ($0 < \delta < 2$) [57] layers with improved metallic character promotes its outstanding HER

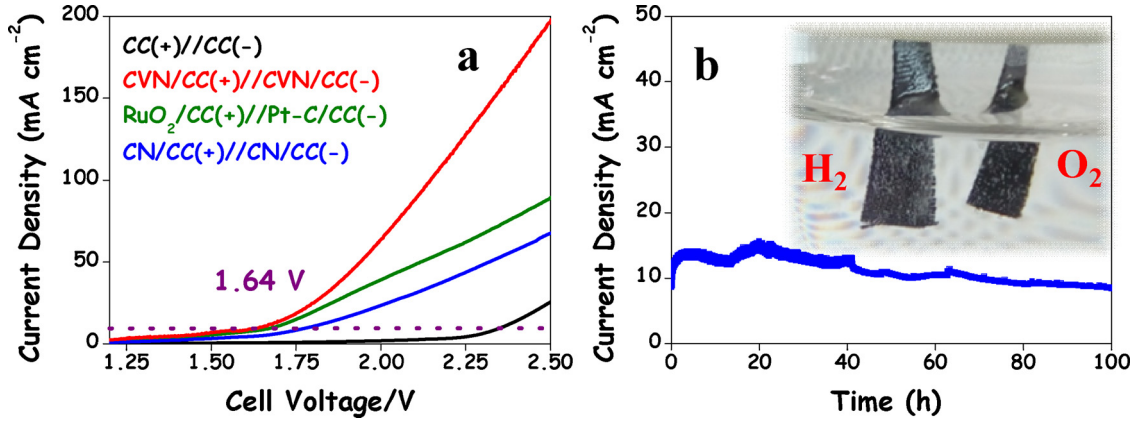

Fig. 5. (a) LSV profiles for various electrocatalysts studied in two-electrode electrolyzer in 1.0 M aqueous KOH solution, (b) CA test by CVN/CC at 1.65 V in two electrode electrolyzer (Inset: Digital image of water splitting by the same CVN/CC electrode as both anode and cathode).

activity in alkaline medium. In contrary to the metallic hydroxides as starting electrocatalyst, the bimetallic nitride provides lower charge transfer resistance, better conductivity, favourable reaction kinetics which have been reflected in its excellent bifunctionality performance in alkaline solution.

4. Conclusion

A facile synthetic method has been demonstrated for the polyaniline (PANI) derived cobalt nitride-vanadium oxynitride nanohybrid on carbon cloth (CVN/CC) for the electrochemical overall water splitting. Instead of common nitridation practice by using toxic gaseous ammonia, the PANI induced synthetic process is risk-free and found to be advantageous due to the formation of nitrogen doped carbon layers in between the active catalyst and conductive support as facile and continuous corridor for electron/charge transportation in the whole electrocatalyst. Moreover, incorporation of vanadium oxynitride into the self-supported Co_4N electrocatalyst plays the important role to generate large number of suitable active sites which significantly enhance the water splitting activity of CVN/CC and even suppress the integrated state-of-the-art Pt-C and RuO_2 electrocatalysts in terms of both efficiency and durability. Finally, this work provides a step forward to the designing of a transition metal nitride-oxynitride hybrid for low-cost, efficient and highly durable water splitting electrocatalyst system for industrial application.

Acknowledgements

This work was supported by a grant from the Basic Science Research Program through the National Research Foundation of Korea (NRF) funded by the Ministry of Science, ICT (2016R1C1B2007299) and the Research Institute of Industrial Science, Hanyang University, Seoul, 133-791, Korea.

Appendix A. Supplementary data

Supplementary material related to this article can be found, in the online version, at doi:https://doi.org/10.1016/j.apcatb.2018.09.061.

Details of materials and characterizations, FESEM image, XRD analysis, XPS spectra, TEM analysis, EIS plots, CA test, LSV curves, C_{dl} calculation, ICP-OES results, table for comparative account on water splitting performance.

References

[1] J.A. Turner, Science 305 (2004) 972–974.
[2] H.T. Wang, H.W. Lee, Y. Deng, Z.Y. Lu, P.C. Hsu, Y.Y. Liu, D.C. Lin, Y. Cui, Nat. Commun. 6 (2015) 7261.
[3] Y.P. Zhu, C. Guo, Y. Zheng, S.-Z. Qiao, Acc. Chem. Res. 50 (2017) 915–923.
[4] I. Roger, M.A. Shipman, M.D. Symes, Nat. Rev. Chem. 1 (2017) 0003.
[5] M.S. Burke, S. Zou, L.J. Enman, J.E. Kellon, C.A. Gabor, E. Pledger, S.W. Boettcher, J. Phys. Chem. Lett. 6 (2015) 3737–3742.
[6] Y. Shi, B. Zhang, Chem. Soc. Rev. 45 (2016) 1529–1541.
[7] E.A. Hernandez-Pagan, N.M. Vargas-Barbosa, T. Wang, Y. Zhao, E.S. Smotkin, T.E. Mallouk, Energy Environ. Sci. 5 (2012) 7582–7589.
[8] J. Chang, Q. Lv, G. Li, J. Ge, C. Liu, W. Xing, Appl. Catal. B 204 (2017) 486–496.
[9] S. Anantharaj, S. Rao Ede, K. Sakthikumar, K. Karthick, S. Mishra, S. Kundu, ACS Catal. 6 (2016) 8069–8097.
[10] S. Dutta, A. Indra, Y. Feng, T. Song, U. Paik, ACS Appl. Mater. Interfaces 9 (2017) 33766–33774.
[11] H. Yin, C.Z. Zhang, F. Liu, Y.L. Hou, Adv. Funct. Mater. 24 (2014) 2930–2937.
[12] J. Xie, Y. Xie, Chem. Eur. J. 22 (2016) 3588–3598.
[13] D. Shu, H. Cheng, C. Lv, M.A. Asi, L. Long, C. He, X. Zou, Z. Kang, Int. J. Hydrogen Energy 39 (2014) 16139–16150.
[14] S. Wirth, F. Harnisch, M. Weinmann, U. Schröder, Appl. Catal. B 126 (2012) 225–230.
[15] Y. Zhang, B. Ouyang, J. Xu, G. Jia, S. Chen, R.S. Rawat, H.J. Fan, Angew. Chem. Int. Ed. 55 (2016) 8670–8674.
[16] P. Chen, K. Xu, Z. Fang, Y. Tong, J. Wu, X. Lu, X. Peng, H. Ding, C. Wu, Y. Xie, Angew. Chem. Int. Ed. 54 (2015) 14710–14714.
[17] F. Meng, H. Zhong, D. Bao, J. Yan, X. Zhang, J. Am. Chem. Soc. 138 (2016) 10226–10231.
[18] K. Xu, P. Chen, X. Li, Y. Tong, H. Ding, X. Wu, W. Chu, Z. Peng, C. Wu, Y. Xie, J. Am. Chem. Soc. 137 (2015) 4119–4125.
[19] F. Yu, H. Zhou, Z. Zhu, J. Sun, R. He, J. Bao, S. Chen, Z. Ren, ACS Catal. 7 (2017) 2052–2057.
[20] D. Gao, J. Zhang, T. Wang, W. Xiao, K. Tao, D. Xue, J. Ding, J. Mater. Chem. A 4 (2016) 17363–17369.
[21] K. Ojha, S. Saha, B. Kumar, K.S. Hazra, A.K. Ganguli, ChemCatChem 8 (2016) 1218–1225.
[22] Y. Zhang, B. Ouyang, J. Xu, S. Chen, R.S. Rawat, H.J. Fan, Adv. Energy Mater. 6 (2016) 1600221.
[23] B. Cao, G.M. Veith, J.C. Neuefeind, R.R. Adzic, P.G. Khalifah, J. Am. Chem. Soc. 135 (2013) 19186–19192.
[24] Z.-L. Wang, X.-F. Hao, Z. Jiang, X.-P. Sun, D. Xu, J. Wang, H.-X. Zhong, F.-L. Meng, X.-B. Zhang, J. Am. Chem. Soc. 137 (2015) 15070–15073.
[25] M. Jiang, Y. Li, Z. Lu, X. Sun, X. Duan, Inorg. Chem. Front. 3 (2016) 630–634.
[26] B. Zhang, C. Xiao, S. Xie, J. Liang, X. Chen, Y. Tang, Chem. Mater. 28 (2016) 6934–6941.
[27] Y. Wang, D. Liu, Z. Liu, C. Xie, J. Huo, S. Wang, Chem. Commun. 52 (2016) 12614–12617.
[28] H.B. Tao, L. Fang, J. Chen, H.B. Yang, J. Gao, J. Miao, S. Chen, B. Liu, J. Am. Chem. Soc. 138 (2016) 9978–9985.
[29] K. Fan, H. Chen, Y. Ji, H. Huang, P.M. Claesson, Q. Daniel, B. Philippe, H. Rensmo, F. Li, Y. Luo, L. Sun, Nat. Commun. 7 (2016) 11981.
[30] Y. Qu, M. Yang, J. Chai, Z. Tang, M. Shao, C.T. Kwok, M. Yang, Z. Wang, D. Chua, S. Wang, Z. Lu, H. Pan, ACS Appl. Mater. Interfaces 9 (2017) 5959–5967.
[31] S. Hyun, V. Ahilan, H. Kim, S. Shanmugam, Electrochem. Commun. 63 (2016) 44–47.
[32] B. Ren, D. Li, Q. Jin, H. Cui, C. Wang, J. Mater. Chem. A 5 (2017) 19072–19078.
[33] X. Peng, L. Wang, L. Hu, Y. Li, B. Gao, H. Song, C. Huang, X. Zhang, J. Fu, K. Huo, P.K. Chu, Nano Energy 34 (2017) 1–7.
[34] Y. Wang, S. Tang, S. Vongehr, J.A. Syed, X. Wang, X. Meng, Sci. Rep. 6 (2016) 12883.
[35] Y. Yu, P. Li, X. Wang, W. Gao, Z. Shen, Y. Zhu, S. Yang, W. Song, K. Ding, Nanoscale 8 (2016) 10731–10738.
[36] T. Zhu, J. Zhou, Z. Li, S. Li, W. Si, S. Zhuo, J. Mater. Chem. A 2 (2014) 12545–12551.
[37] Y. Shi, Y. Wang, Y. Yu, Z. Niu, B. Zhang, J. Mater. Chem. A 5 (2017) 8897–8902.
[38] K. Gong, F. Du, Z. Xia, M. Durstock, L. Dai, Science 323 (2009) 760–764.
[39] S. Dutta, C. Ray, Y. Negishi, T. Pal, ACS Appl. Mater. Interfaces 9 (2017) 8134–8141.
[40] Z. Luo, R. Miao, T.D. Huan, I.M. Mosa, A.S. Poyraz, W. Zhong, J.E. Cloud, D.A. Kriz, S. Thanneeru, J. He, Y. Zhang, R. Ramprasad, S.L. Suib, Adv. Energy Mater. 6 (2016) 1600528.
[41] C. Lu, D. Tranca, J. Zhang, F.R. Hernandez, Y. Su, X. Zhuang, F. Zhang, G. Seifert, X. Feng, ACS Nano 11 (2017) 3933–3942.
[42] D.K. Singh, R.N. Jenjeti, S. Sampath, M. Eswaramoorthy, J. Mater. Chem. A 5 (2017) 6025–66031.
[43] S. Jing, L. Zhang, L. Luo, J. Lu, S. Yin, P.K. Shen, P. Tsiakaras, Appl. Catal. B 224 (2018) 533–540.
[44] H. Shi, H. Liang, F. Ming, Z. Wang, Angew. Chem. Int. Ed. 56 (2017) 573–577.
[45] T. Tang, W.-J. Jiang, S. Niu, N. Liu, H. Luo, Y.-Y. Chen, S.-F. Jin, F. Gao, L.-J. Wan, J.-S. Hu, J. Am. Chem. Soc. 139 (2017) 8320–8328.
[46] J. Wang, H.-x. Zhong, Z.-l. Wang, F.-l. Meng, X.-b. Zhang, ACS Nano 10 (2016) 2342–2348.
[47] Y. Hou, M.R. Lohe, J. Zhang, S. Liu, X. Zhuang, X. Feng, Energy Environ. Sci. 9 (2016) 478–483.
[48] M. Ledendecker, S.K. Calderýn, C. Papp, H.-P. Steinrîck, M. Antonietti, M. Shalom, Angew. Chem. Int. Ed. 54 (2015) 12361–12365.
[49] X.-D. Wang, H.-Y. Chen, Y.-F. Xu, J.-F. Liao, B.-X. Chen, H.-S. Rao, D.-B. Kuang, C.-Y. Su, J. Mater. Chem. A 5 (2017) 7191–7199.
[50] N. Xu, G. Cao, Z. Chen, Q. Kang, H. Dai, P. Wang, J. Mater. Chem. A 5 (2017) 12379–12384.
[51] C. Wang, J. Jiang, T. Ding, G. Chen, W. Xu, Q. Yang, Adv. Mater. Interfaces 3 (2016) 1500454.
[52] C. Xiao, Y. Li, X. Lu, C. Zhao, Adv. Funct. Mater. 26 (2016) 3515–3523.
[53] X. Gao, H. Zhang, Q. Li, X. Yu, Z. Hong, X. Zhang, C. Liang, Z. Lin, Angew. Chem. Int. Ed. 55 (2016) 6290–6294.
[54] W. Li, S. Zhang, Q. Fan, F. Zhang, S. Xu, Nanoscale 9 (2017) 5677–5685.
[55] Y. Hou, M. Qiu, G. Nam, M.G. Kim, T. Zhang, K. Liu, X. Zhuang, J. Cho, C. Yuan, X. Feng, Nano Lett. 17 (2017) 4202–4209.
[56] A. Indra, P.W. Menezes, C. Das, C. Gobel, M. Tallarida, D. Schmeiber, M.A. Driess, J. Mater. Chem. A 5 (2017) 5171–5177.
[57] T. Liu, M. Li, C. Jiao, M. Hassan, X. Bo, M. Zhou, H.-L. Wang, J. Mater. Chem. A 5 (2017) 9377–9390.
[58] N.S. McIntyre, M.G. Cook, Anal. Chem. 47 (1975) 2208–2213.
[59] J. Tian, Q. Liu, A.M. Asiri, X. Sun, J. Am. Chem. Soc. 136 (2014) 7587–7590.
[60] G.K. Veerasubramani, A. Chandrasekhar, M.S.P. Sudhakaran, Y.S. Mok, S.J. Kim, J. Mater. Chem. A 5 (2017) 11100–11113.
[61] M.J. Kim, S. Kim, D. Song, S.K. Oh, K.J. Chang, E.A. Cho, Appl. Catal. B 227 (2018) 340–348.
[62] X. Zhao, X. Li, Y. Yan, Y. Xing, S. Lu, L. Zhao, S. Zhou, Z. Peng, J. Zeng, Appl. Catal. B 236 (2018) 569–575.